IN AIR 2019
12 - 13 November 2019, Budapest

8th International Conference on Air Transport – INAIR 2019
GLOBAL TRENDS IN AVIATION

Damian Olejniczak

Poznan University of Technology

Institute of Combustion Engines and Transport

Faculty of Transport Engineering

Analysis of thermodynamic parameters of the air at the airfoil stagnation point in the aspect of the icing process initiation

E-mail address: damian.a.olejniczak@doctorate.put.poznan.pl

12.11.2019

Presentation plan:

Introduction

- the aircraft icing definition
- conditions conductive to aircraft icing
- the shape and structure of icing on the surface of the aircraft wing
- the effect of icing on the aircraft's flight characteristics

Methodology

- wing models
- CFD simulation conditions

Results

- the values of thermodynamic parameters of air within the stagnation point depending on the flight velocity v and flight altitude H based on CFD tests under ISA standard atmosphere conditions.
- model determining the air temperature within the stagnation point of the airfoil depending on the flight parameters of the aircraft: flight velocity v, flight altitude H, parameters of the ISA standard atmosphere and individual geometric characteristics of the airfoils.

Conclusions

The aircraft icing definition:

The phenomenon of aircraft icing is defined as the process of changing the concentration of water contained in the air in the form of steam into a solid form accumulating on the elements of the aircraft structure

Two types of aircraft icing:

engine icing

aircraft structure icing

One of the most common cause of air accidents in the category of accidents caused by bad weather conditions

The number of accidents of General Aviation aircraft and planes with MTOM<2250 kg in 2012-2016 on the basis of Annual Safety Review published by EASA

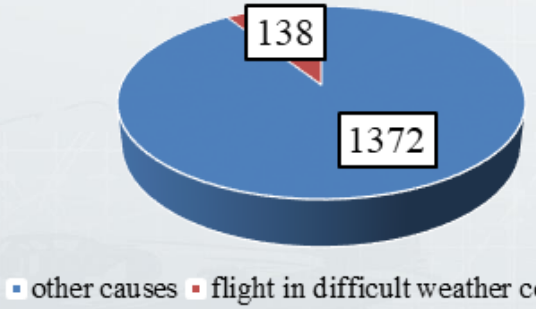

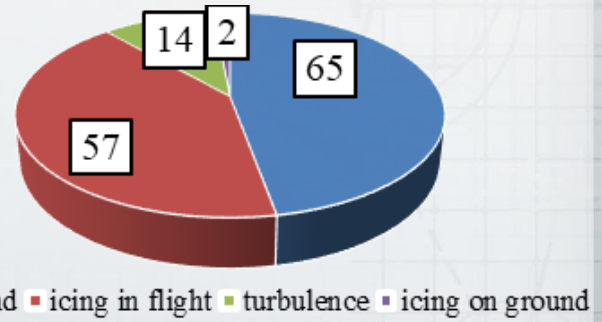

Conditions conductive to aircraft icing

Two types of aircraft icing:

engine icing

air temperature

< 10°C

aircraft structure icing

air temperature

< 0°C

high air humidity

presence of water in the atmosphere in all forms, clouds, precipitation, overflowing water

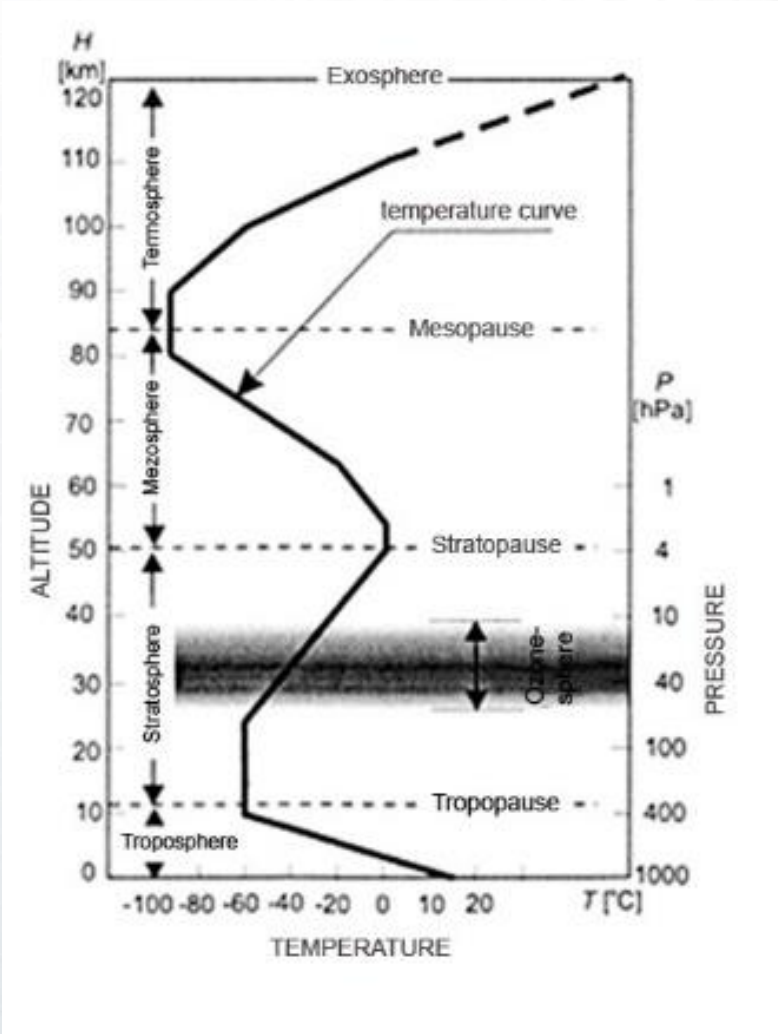

The shape and structure of icing on the surface of the aircraft wing

Solid

Profile

Mixed

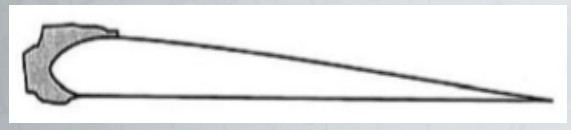

+

The effect of icing on the aircraft's flight characteristics

- Mass of aircraft G ↑ increase
- Drag force F_D ↑ increase
- Lift force coefficient C_L ↓ reduction
- Lift force F_L ↓ reduction
- Mass flow rate in engine inlet ↓ reduction
- Engine power, engine thrust F_T ↓ reduction

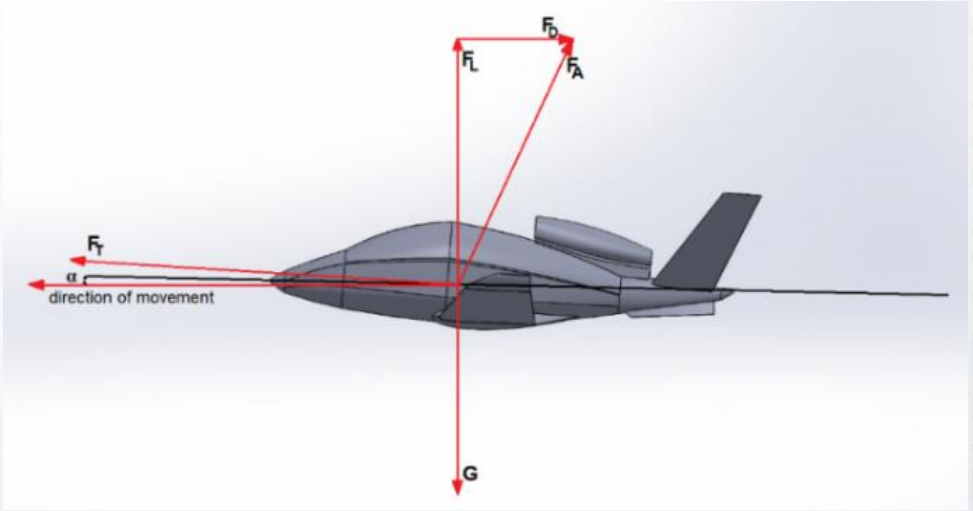

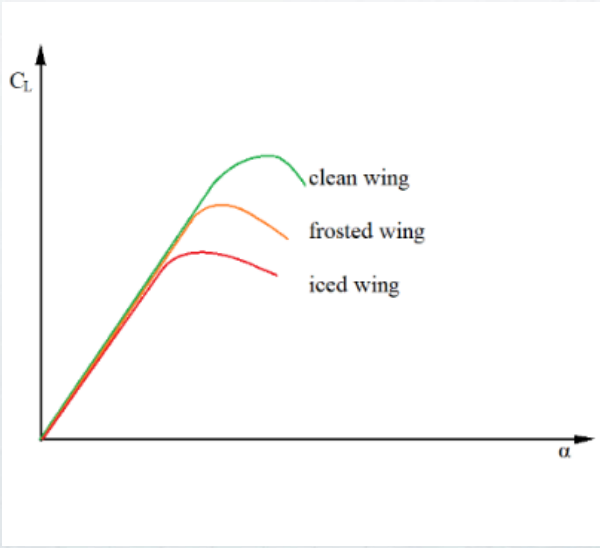

Methodology: wing models

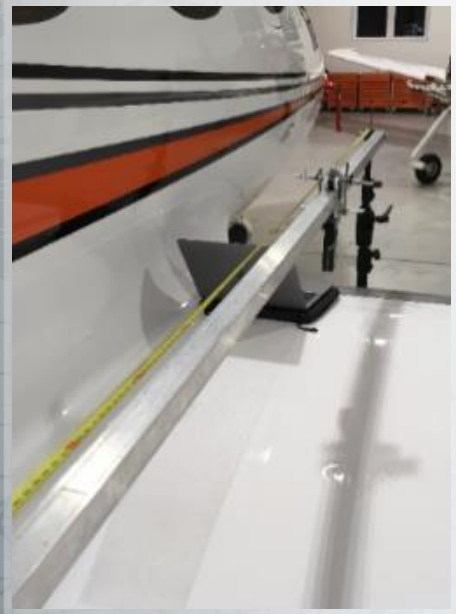

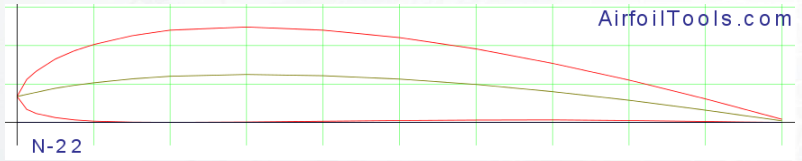

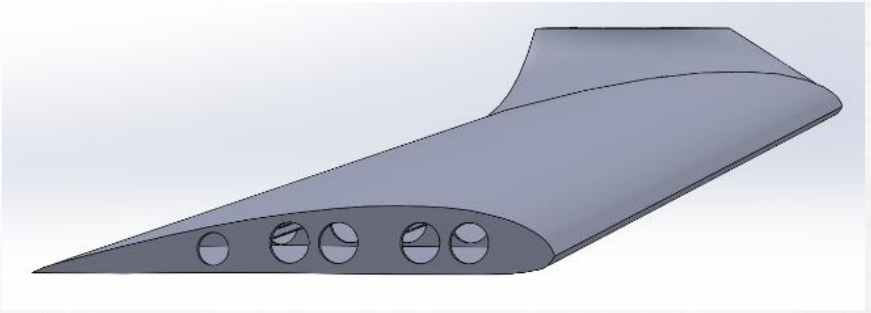

N-22 airfoil

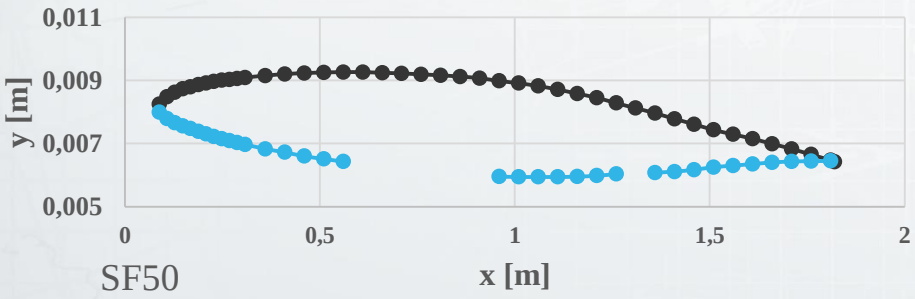

SF50

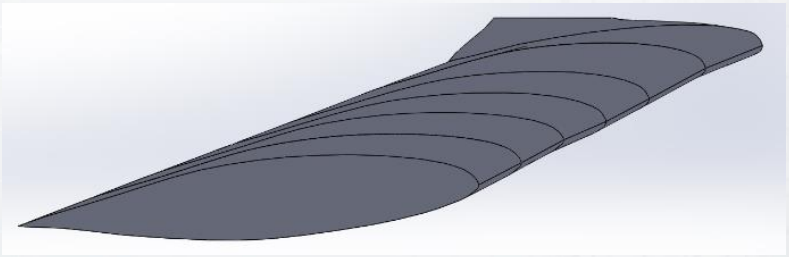

Cirrus SF-50 Vision Jet airfoil

The characteristic dimensions of the wings are:
the length of the wing **L=5,4 [m]**, the root chord **c_R=2 [m]**, the tip chord **c_T= 1,4 [m]**,
the taper ratio **$\lambda=c_T/c_R=0,7$**, the mean aerodynamic chord **$c_M=2\cdot c_R\cdot(1+\lambda+\lambda^2)/(3\cdot(1+\lambda))=1,718$ [m]**,
dihedral angle **$\beta=7,4^\circ$**

Methodology: simulation conditions

- numerical simulations were performed under ISA conditions for selected aircraft flight velocity
- CFD tests assumed a universal angle of attack $\alpha=4^{\circ}$
- the simulation model used was the turbulent k-epsilon model for compressible gas
- the model's mesh was set using the automatic function tools to the 1 setting

No.	Aircraft velocity v [m/s]	Flight altitude H [m]	Air temperature T_A [K]	Air pressure P_A [Pa]	Air density ρ_A [kg/m^3]	Dynamic viscosity μ [10^{-5} N·s/m^2]	Kinematic viscosity ν [10^{-5} m^2/s]	Reynolds number $Re=(c_M \cdot v)/\nu$
1	40	0	288	101 325	1,225	1,789	1,460	4 706 849,32
2	50	0	288	101 325	1,225	1,789	1,460	5 883 561,64
3	60	0	288	101 325	1,225	1,789	1,460	7 060 273,97
4	70	0	288	101 325	1,225	1,789	1,460	8 236 986,30
5	80	0	288	101 325	1,225	1,789	1,460	9 413 698,63
6	40	1 000	282	89 867	1,112	1,758	1,581	4 346 616,07
7	50	1 000	282	89 867	1,112	1,758	1,581	5 433 270,08
8	60	1 000	282	89 867	1,112	1,758	1,581	6 519 924,10
9	70	1 000	282	89 867	1,112	1,758	1,581	7 606 578,12
10	80	1 000	282	89 867	1,112	1,758	1,581	8 693 232,13
11	40	3 000	269	70 089	0,909	1,694	1,864	3 686 695,28
12	50	3 000	269	70 089	0,909	1,694	1,864	4 608 369,10
13	60	3 000	269	70 089	0,909	1,694	1,864	5 530 042,92
14	70	3 000	269	70 089	0,909	1,694	1,864	6 451 716,74
15	80	3 000	269	70 089	0,909	1,694	1,864	7 373 390,56
16	40	5 000	256	53 994	0,736	1,628	2,212	3 106 690,78
17	50	5 000	256	53 994	0,736	1,628	2,212	3 883 363,47
18	60	5 000	256	53 994	0,736	1,628	2,212	4 660 036,17
19	70	5 000	256	53 994	0,736	1,628	2,212	5 436 708,86
20	80	5 000	256	53 994	0,736	1,628	2,212	6 213 381,56

Methodology: simulation mesh

- The mesh of the N-22 wing model is made of 297 383 nodes, of which 290 981 are fluid nodes, and 6 402 solid nodes
- The mesh of the SF50 wing model consists of 228 551 nodes, of which 223 510 are fluid nodes, and 5041 solid nodes

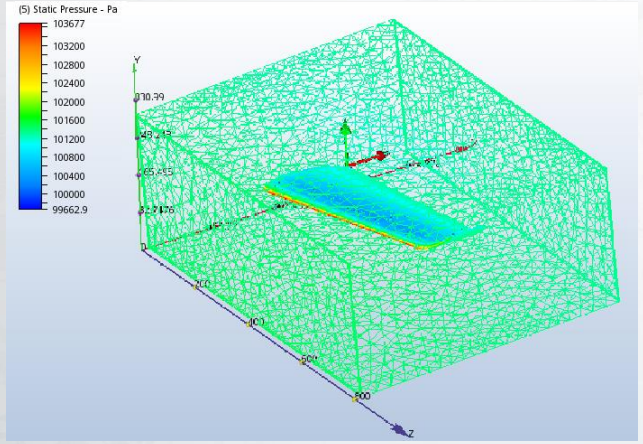

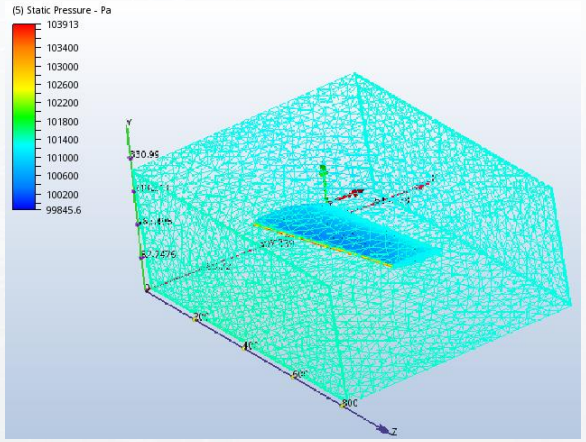

The area within the stagnation point was defined as a sphere with radius r=0.01 [m] in which n=500 measurements of selected thermodynamic parameters were made. The test results are presented as average values from n=500 measurements of thermodynamic parameters of air within the stagnation point

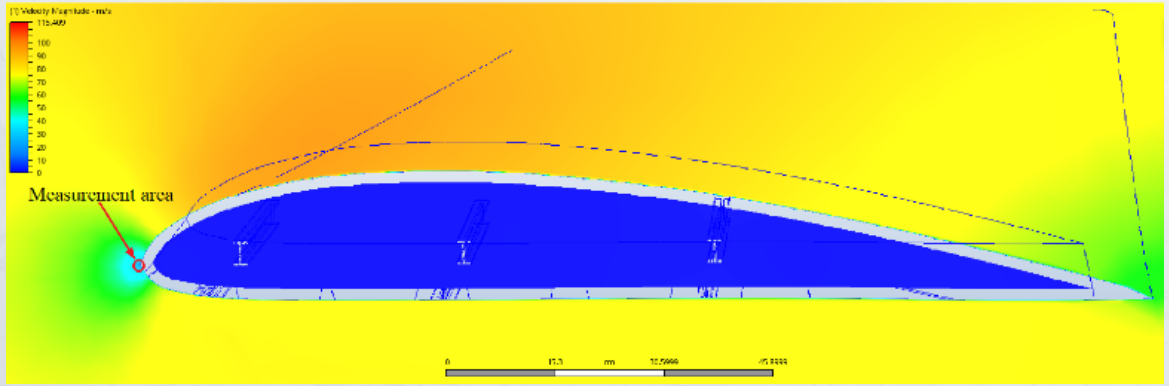

Results

N-22						SF50					
H [m]	v [m/s]	Δv [m/s]	ΔP [Pa]	ΔT [K]	Δρ [kg/m3]	H [m]	v [m/s]	Δv [m/s]	ΔP [Pa]	ΔT [K]	Δρ [kg/m3]
	40	-27,721	1333,384	0,712	0,013		40	-28,563	1581,445	0,722	0,016
	50	-34,835	2050,604	1,115	0,020		50	-33,424	2129,816	1,098	0,021
0	60	-41,041	2929,697	1,594	0,028	0	60	-40,750	3016,493	1,592	0,030
	70	-48,497	4108,677	2,178	0,040		70	-47,338	3951,999	2,165	0,038
	80	-54,830	5279,984	2,831	0,051		80	-55,056	5669,845	2,847	0,056
	40	-28,084	1224,253	0,718	0,012		40	-26,669	1388,004	0,702	0,014
	50	-34,434	1885,009	1,108	0,019		50	-32,833	1900,897	1,088	0,019
1000	60	-41,475	2703,673	1,606	0,027	1000	60	-42,001	2906,795	1,618	0,029
	70	-48,003	3696,437	2,170	0,037		70	-48,653	3776,298	2,194	0,038
	80	-55,258	4751,067	2,848	0,047		80	-55,122	4999,518	2,858	0,050
	40	-27,387	987,390	0,708	0,010		40	-27,635	1062,072	0,713	0,011
	50	-34,582	1530,773	1,113	0,016		50	-33,985	1589,327	1,106	0,017
3000	60	-41,537	2222,649	1,605	0,023	3000	60	-42,771	2397,035	1,630	0,025
	70	-50,007	3138,232	2,214	0,033		70	-46,697	2961,791	2,147	0,031
	80	-55,463	3947,327	2,850	0,041		80	-55,484	4119,235	2,861	0,043
	40	-26,696	764,476	0,698	0,008		40	-28,062	818,968	0,719	0,009
	50	-34,637	1259,909	1,111	0,014		50	-32,285	1209,897	1,076	0,013
5000	60	-41,905	1815,699	1,610	0,020	5000	60	-41,791	1903,928	1,613	0,021
	70	-47,571	2395,098	2,162	0,026		70	-49,106	2486,188	2,200	0,027
	80	-55,970	3254,596	2,865	0,036		80	-56,024	3348,226	2,878	0,037

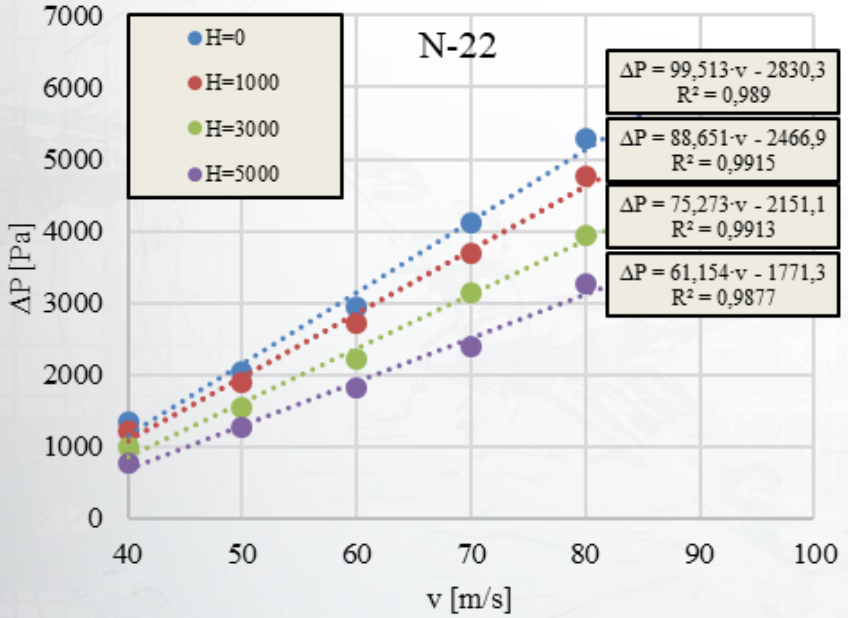
N-22
H=0
H=1000
H=3000
H=5000
ΔP = 99,513·v - 2830,3
R² = 0,989
ΔP = 88,651·v - 2466,9
R² = 0,9915
ΔP = 75,273·v - 2151,1
R² = 0,9913
ΔP = 61,154·v - 1771,3
R² = 0,9877
ΔP [Pa]
v [m/s]

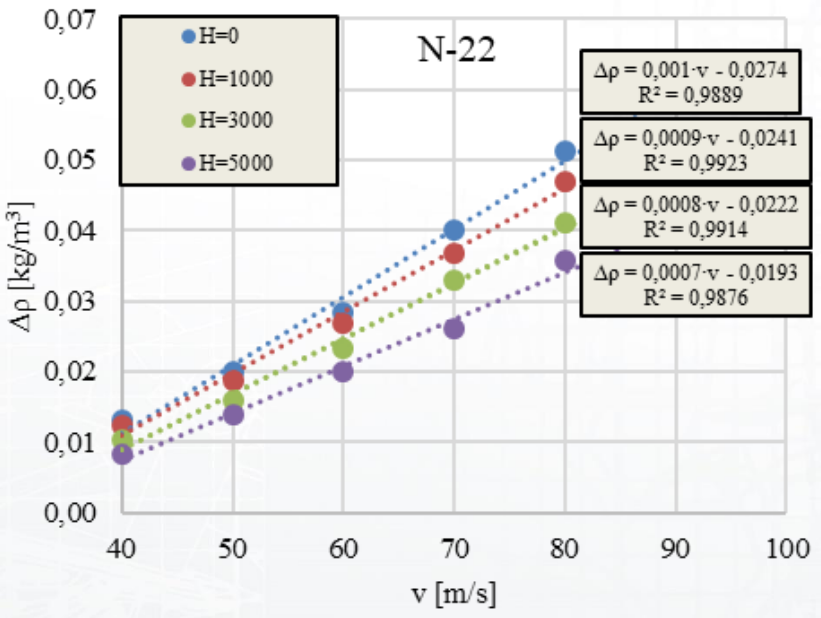
N-22
H=0
H=1000
H=3000
H=5000
Δρ = 0,001·v - 0,0274
R² = 0,9889
Δρ = 0,0009·v - 0,0241
R² = 0,9923
Δρ = 0,0008·v - 0,0222
R² = 0,9914
Δρ = 0,0007·v - 0,0193
R² = 0,9876
Δρ [kg/m³]
v [m/s]

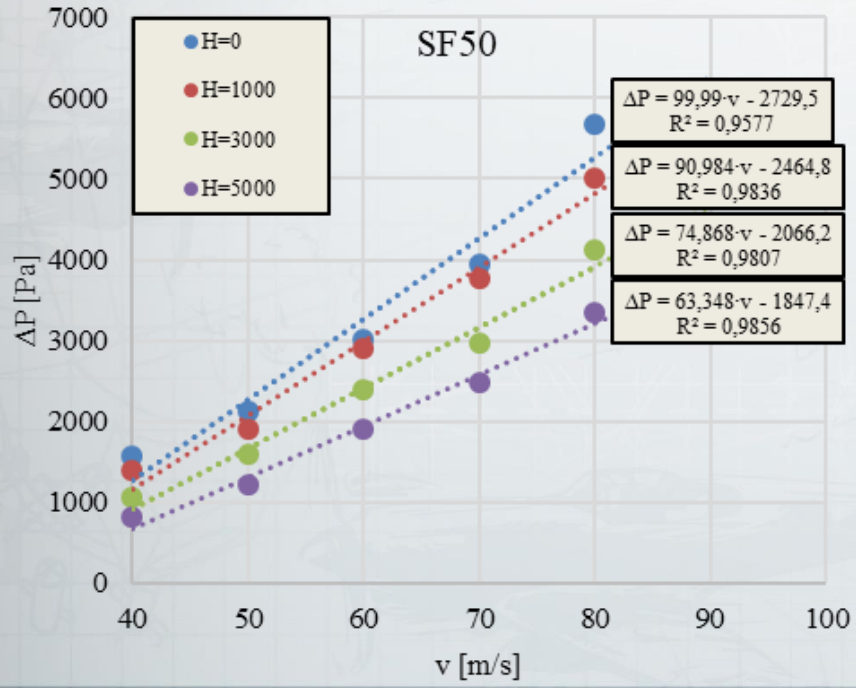
SF50
H=0
H=1000
H=3000
H=5000
ΔP = 99,99·v - 2729,5
R² = 0,9577
ΔP = 90,984·v - 2464,8
R² = 0,9836
ΔP = 74,868·v - 2066,2
R² = 0,9807
ΔP = 63,348·v - 1847,4
R² = 0,9856
ΔP [Pa]
v [m/s]

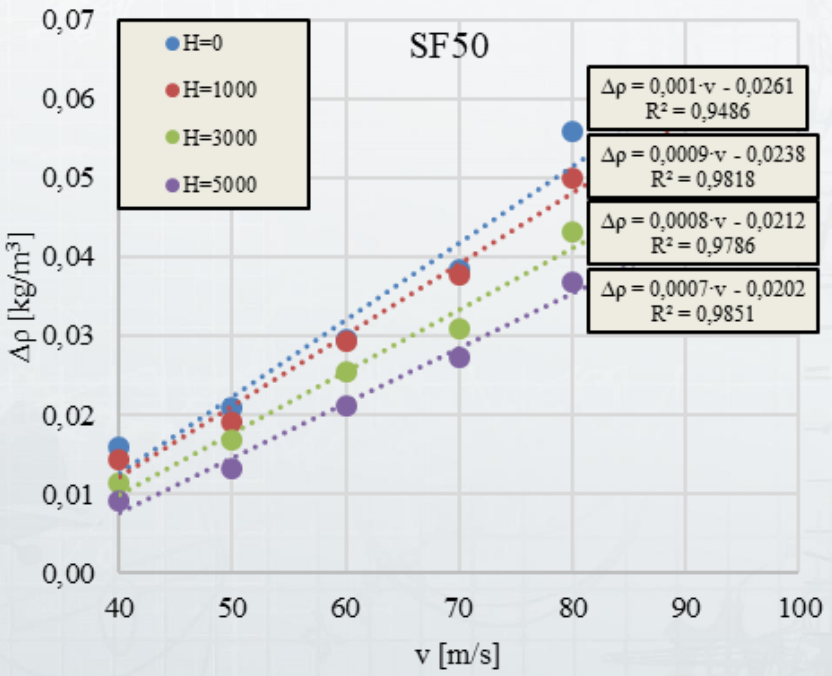
SF50
H=0
H=1000
H=3000
H=5000
Δρ = 0,001·v - 0,0261
R² = 0,9486
Δρ = 0,0009·v - 0,0238
R² = 0,9818
Δρ = 0,0008·v - 0,0212
R² = 0,9786
Δρ = 0,0007·v - 0,0202
R² = 0,9851
Δρ [kg/m³]
v [m/s]

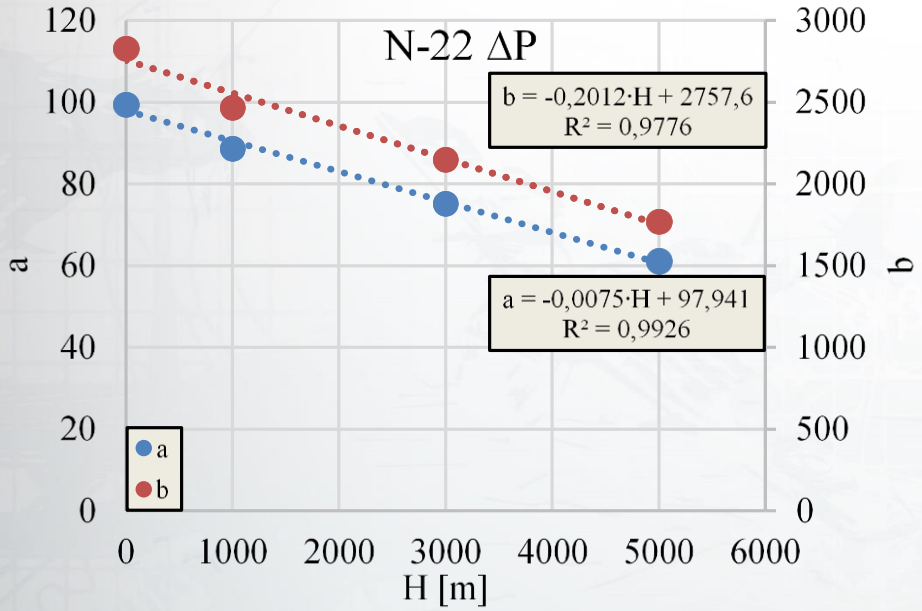
N-22 ΔP
b = -0,2012·H + 2757,6
R² = 0,9776
a = -0,0075·H + 97,941
R² = 0,9926
a
b
H [m]

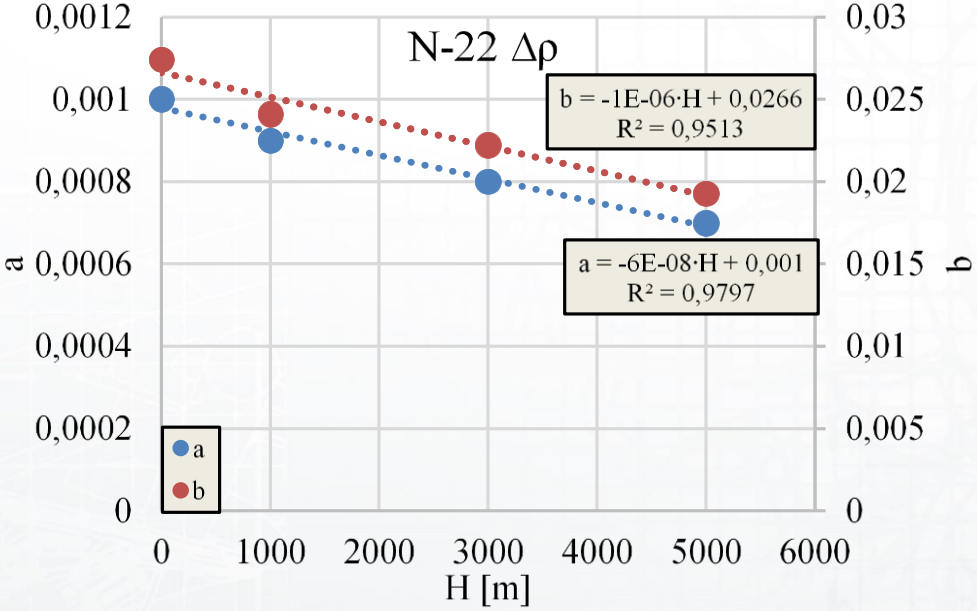
N-22 Δρ
b = -1E-06·H + 0,0266
R² = 0,9513
a = -6E-08·H + 0,001
R² = 0,9797
a
b
H [m]

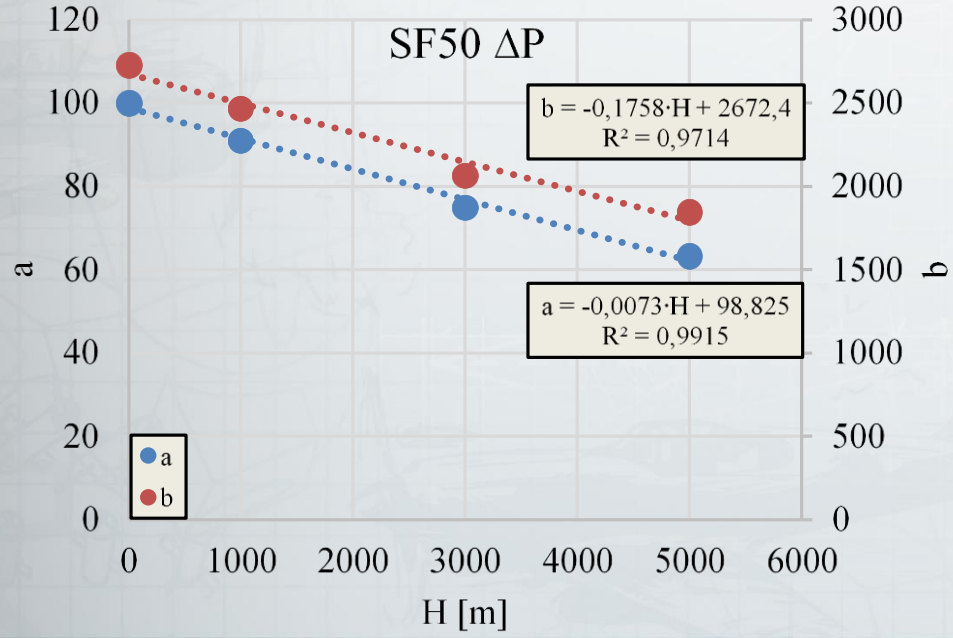
SF50 ΔP
b = -0,1758·H + 2672,4
R² = 0,9714
a = -0,0073·H + 98,825
R² = 0,9915
a
b
H [m]

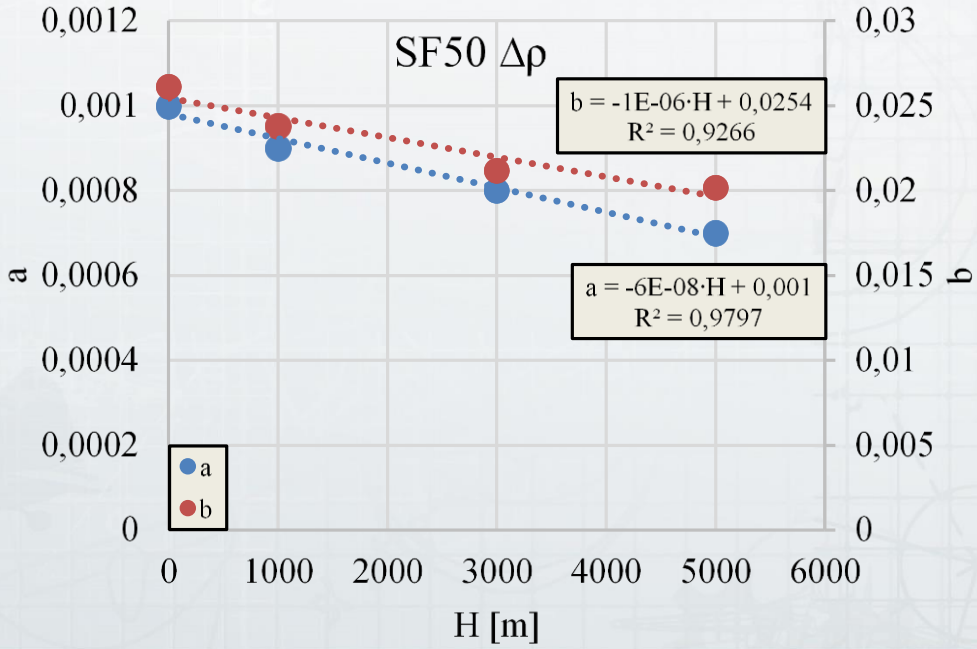
SF50 Δρ
b = -1E-06·H + 0,0254
R² = 0,9266
a = -6E-08·H + 0,001
R² = 0,9797
a
b
H [m]

Model determining the air temperature within the stagnation point of the airfoil

$$T_{SP} = \frac{P_A f(H) + \Delta P f(\mathrm{v}, H)}{(\rho_A f(H) + \Delta \rho f(\mathrm{v}, H)) \cdot R},$$

$$T_{SP.N-22} = \frac{P_0 \cdot (1 - \frac{H}{44300})^{5,256} + ((-0,0075 \cdot H + 97,941) \cdot \mathrm{v} - (-0,2012 \cdot H + 2757,6))}{(\rho_0 \cdot (1 - \frac{H}{44300})^{4,256} + ((-6 \cdot 10^{-8} \cdot H + 0,001) \cdot \mathrm{v} - (-1 \cdot 10^{-6} \cdot H + 0,0266)) \cdot R},$$

$$T_{SP.SF50} = \frac{P_0 \cdot (1 - \frac{H}{44300})^{5,256} + ((-0,0073 \cdot H + 98,825) \cdot \mathrm{v} - (-0,1758 \cdot H + 2672,4))}{(\rho_0 \cdot (1 - \frac{H}{44300})^{4,256} + ((-6 \cdot 10^{-8} \cdot H + 0,001) \cdot \mathrm{v} - (-1 \cdot 10^{-6} \cdot H + 0,0254)) \cdot R},$$

where:

- T_{SP} – temperature within the airfoil stagnation point [K],
- $P_A f(H)$ – atmospheric air pressure as a function of altitude H based on the ISA standard atmosphere [Pa],
- $\Delta P f(\mathrm{v}, H)$ – pressure increase at the point of stagnation depending on the aircraft velocity v and flight altitude H [Pa],
- $\rho_A f(H)$ – air density as a function of altitude H based on the ISA standard atmosphere [kg/m^3],
- $\Delta \rho f(\mathrm{v}, H)$ – air density increase at the point of stagnation depending on the aircraft velocity v and flight altitude H [kg/m^3],
- R – specific gas constant for dry air, R =286,9 [J/(kg·K)],
- P_0 – ambient pressure on standard mean sea level, P_0 =101 325 [Pa],
- ρ_0 – ambient density on standard mean sea level, ρ_0 =1,2255 [kg/m^3],
- H – aircraft flight altitude [m],
- v – aircraft velocity [m/s].

Conclusions

- The model elements associated with the standard atmosphere parameters can be replaced by real values of individual thermodynamic parameters of air occurring at a given flight level, however, remembering about increasing the estimation inaccuracy in this way.
- Estimated TSP<273.15 [K] under the given flight conditions of the aircraft indicate that conditions are favorable to icing the airfoil. When assessing conditions conducive to icing, it is also necessary to take into account the humidity of the air omitted in the analysis. Knowing the air humidity and the estimated air temperature at the point of stagnation, it is possible to diagnose the conditions for initiating the icing process.
- On the basis of the determined functional dependences describing the values of increments of thermodynamic parameters of air within the stagnation point, one can observe slight differences in the values of linear function coefficients describing the airfoils. These differences indicate the minimal effect of geometrical features of airfoils on the value of increments of thermodynamic parameters within the stagnation point.
- The estimation error between the values of the temperature increase ΔT determined during the CFD tests and the TSP values estimated on the basis of the developed model does not exceed 10%.
- The developed model is designed in the future to analyze the effect of air humidity on the TSP value of the airfoil and validation in future wind tunnel tests. Also needed to determine at which temperatures and humidity a certain airfoil icing occurs.

Bibliography

Antonini, C., Innocenti, M., Horn, T., Marengo, M., Amirfazli, A., 2011. Understanding the effect of superhydrophobic coatings on energy reduction in anti-icing systems. Cold Regions Science and Technology. Volume: 67. Issue: 1−2. Pages: 58−67. DOI: 10.1016/j.coldregions.2011.02.006.

Boudala, F., Isaac, GA., Wu, D., 2019. Aircraft icing study using integrated observations and model data. Weather and Forecasting. Volume: 34. Issue: 3. Pages: 485−506. DOI: 10.1175/WAF-D-18-0037.1.

Bragg, MB., Gregorek, GM., Lee, JD., 1986. Airfoil aerodynamics in icing conditions. Journal of Aircraft. Volume: 23. Issue: 1. Pages: 76−81. DOI: 10.2514/3.45269.

Cebeci, T., Kafyeke, F., 2003. Aircraft icing. Annual Review of Fluid Mechanics. Volume: 35. Pages: 11−21. DOI: 10.1146/annurev.fluid.35.101101.161217.

Chachurski, R., Waślicki, P., 2011. Wykrywanie i sygnalizacja oblodzenia statków powietrznych. Prace Instytutu Lotnictwa 213. Warszawa.

Gębura, A., Janusiak, K., Paradowski, M., 2014. Oblodzenie statku powietrznego – przyczyny, skutki, przeciwdziałanie. Journal of KONBiN 4(32)2014. ISSN 1895-8281. DOI 10.2478.

Jasinski, R., 2018. Mass and number analysis of particles emitted during aircraft landing. E3S Web Of Conferences. Volume 44. DOI: 10.1051/E3SCONF/20184400057

Jasinski, R., 2019. Particle emission parameter analysis from multirole fighter aircraft engine. IOP Conference Series: Earth And Environmental Science. Volume 2014. DOI: 10.1088/1755-1315/214/1/012011

Jasinski, R., Markowski, J., Pielecha, J., 2017. Probe positioning for the exhaust emissions measurements. Procedia Engineering. Volume: 192. Pages 381−386. DOI: 10.1016/J.PROENG.2017.06.066

Lewitowicz, J., Żyluk, A., 2006. Podstawy eksploatacji statków powietrznych. TOM 5. Wydawnictwo Instytutu Technicznego Wojsk Lotniczych. Warszawa.

Liu, Y., Ma, LQ., Wang, W., Kota, AK., 2018. An experimental study on soft PDMS materials for aircraft icing mitigation. Applied Surface Science. Volume: 447. Pages: 599−609. DOI: 10.1016/j.apsusc.2018.04.032.

Markowski, J., Pielecha, J., Jasinski, R., 2017. Model to assess the exhaust emissions from the engine of a small aircraft during flight. Procedia Engineering. Volume: 192. Pages 557−562. DOI: 10.1016/J.PROENG.2017.06.096

Milkiewicz, A., Stepaniuk, R., 2009. Praktyczna aerodynamika i mechanika lotu samolotu odrzutowego, w tym wysokomanewrowego. Wydawnictwo Instytutu Technicznego Wojsk Lotniczych. Warszawa.

Szewczak, P., 2007. Meteorologia dla pilota samolotowego (PPL, CPL, ATPL, IR). Seria szkoleniowa ,,AVIA-TEST''. Poznań.

Szutowski, L., 2007. Poradnik pilota samolotowego. Seria szkoleniowa ,,AVIA-TEST''. Poznań.

http://airfoiltools.com/airfoil. access 20.05.2019.

https://www.easa.europa.eu/document-library/general-publications?publication_type%5B%5D=144. Annual Safety Review 2012-2016. access 20.05.2019.

Thank you for your attention